ES Energy & Environment

RESEARCH PAPER

View Article Online

Extremely Low Thermal Conductivity of Graphene Nanoplatelets Using Nanoparticle Decoration

Lin Qiu,[1,2] Pu Guo,[1,2] Hanying Zou,[1,2] Yanhui Feng,[1,2,*] Xinxin Zhang,[1,2] Shahid Pervaiz[3] and Dongsheng Wen[3]

Stacking thin graphene layers into three-dimensional (3D) microscopic structure named graphene nanoplatelets (GNPs) could render much lower thermal conductivity (κ) compared with single-layer graphene with ultrahigh κ of around 5000 $W \cdot m^{-1} \cdot K^{-1}$. In this study, decorating GNP surface with nanoparticles (NPs) is proposed to be an effective approach to further push down the lower limit value of κ for GNPs. By introducing six metallic and non-metallic NPs, *i.e.*, Au, Ag, Cu, Fe, Al_2O_3 and SiO_2 NPs onto the GNP surface, we experimentally corroborate that the κ values of GNP stacking powders approaches to 0.07 $W \cdot m^{-1} \cdot K^{-1}$, which is 10^5 magnitudes lower than that of ideal 2D graphene materials. This remarkable reduction could be ascribed to the greatly limited sizes of ideal 2D lattice structure (~2 μm) together with random stacking arrangement and extra phonon scattering sites due to the introduction of heterogeneous NPs. Significantly, it is demonstrated that even distribution and small diameter of NPs are beneficial to thermal transport of stacking GNPs. The progress made so far could pave way to GNP materials with tunable thermal transport performance.

Keywords: Graphene nanoplatelet; Nanoparticle decoration; Thermal conductivity; Tunable thermal transport

Received 7 August 2018, **Accepted** 5 September 2018

DOI: 10.30919/esee8c139

1. Introduction

As a representative two-dimensional (2D) material, hexagonal honeycomb-structured graphene exhibits unique multi-functional optical, electrical and thermal properties, which attracts a lot of attention nowadays.[1-4] Stacking thin graphene into plate constructs an intriguing three-dimensional (3D) microscopic structure named graphene nanoplatelets (GNPs), which possesses an extremely high specific surface area up to 2630 m^2/g,[5] a low density down to 0.392 g/cm^3 (~ 5 % of the density of steel)[6] and a high electron mobility of 25,000 $cm^2 \cdot V^{-1} \cdot s^{-1}$.[7] It is well-known that a single-layer (SL) graphene generally exhibits ultrahigh thermal conductivity (κ) at room temperature (RT) of around 5000 $W \cdot m^{-1} \cdot K^{-1}$.[8] Owing to the extremely limited number of graphene layers, GNPs render remarkably different physical properties from that of graphite. What is more intriguing is that the GNPs could render much lower κ compared with SL graphene.[9-12] Due to greatly limited sizes of ideal 2D lattice structure (~2 μm)[13] and random stacking arrangement, the magnitude of κ for GNPs can be reduced to 0.2~0.4 W/m K after dispersed into polymer matrices.[14,15] A intriguing question to explore is what is the lower limit value of κ for GNPs.

Loading nanoparticles (NPs) between graphene layers is an effective approach to reduce κ of GNP while maintaining the superior stability, electrical and optical properties of graphene.[16-23] Generally, the remarkable increase in surface energy originating from the size shrinkage enables NPs to agglomerate. The NP agglomerate could move into inter-graphene layer spaces and diminish the interactions between the GNPs. In addition, heterogenous interfacial sites are formed once NPs are loaded onto graphene surface, which cause an extremely high phonon scattering probability and thus limit the thermal transport within GNPs.

Here, the role of NPs in affecting thermal transport of GNPs was explored and discussed by analyzing the κ of various GNP powders decorated with both metallic and non-metallic NPs, *i.e.*, Au, Ag, Cu, Fe, Al_2O_3 and SiO_2 NPs. It was intriguing to find that the values of κ of NP-decorated GNP powders are on the order of 0.1 W/m K, which is extremely lower than the reported high κ of graphene. This observation could be explained by a direct result of numerous fracture interfaces and NP-based extra phonon scattering sites which interrupted the phonon transmission both along and perpendicular to graphene layers. Significantly, it was demonstrated that even distribution and small diameter of NPs were beneficial to thermal transport of stacking GNPs, which could pave way to GNP materials with tunable thermal transport performance.

2. Experimental

2.1 Preparation of NP-decorated GNPs

The NP-decorated GNPs were prepared via the microwave assisted

---

[1] *School of Energy and Environmental Engineering, University of Science and Technology Beijing, Beijing 100083, China*

[2] *Beijing Key Laboratory of Energy Saving and Emission Reduction for Metallurgical Industry,University of Science and Technology Beijing, Beijing 100083, China*

[3] *School of Chemical and Process Engineering, University of Leeds, Leeds LS2 9JT, UK*

[*] ***E-mail:*** *yhfeng@me.ustb.edu.cn*

solvothermal process. Specifically, 20 ml of graphene sample was mixed with the NPs and 10 ml of diethylene glycol, which acted as reducing agent in the chemical reduction process. Six kinds of NPs, *i.e.*, Au NPs (1 ml, 500 ppm), Ag NPs (1 ml, 500 ppm), Fe NPs (1 ml, 500 ppm), Al_2O_3 NPs (0.1 g, 500 ppm), SiO_2 NPs (0.1 g, 500 ppm) and Cu NPs from $CuSO_4$ (0.5 g) were selected to decorate GNP, respectively. In a microwave oven MARS-6, the mixtures were held at 120 °C for 10 min. After that, the samples were allowed to cool down and collected.

2.2 Characterizations

A HITACHI S-4800 field emission scanning electron microscope (FESEM, FEG, FEI, Japan) was used to characterize the sizes and morphologies of the GNPs. A Bruker Multimode-8 Nanoscope atomic force microscope (AFM, Billerica, MA, USA) was used to characterize the thickness of GNP flakes. The crystalline behavior was measured by an X-ray diffractometer using Cu Kα radiation with λ = 1.54184Å (D8 ADVANCE, Bruker AXS, Karlsruhe, Germany). The chemical bonding information was measured by Fourier transform infrared spectrometer (Frontier MIR/NIR + SP10, PerkinElme, Waltham, USA). Raman spectra of different samples under 514, 633 and 785 nm excitation wavelengths were measured by an inVia-Reflex Raman Spectrometer (Renishaw, London, UK).

2.3 Thermal conductivity measurement

The 3ω method-based experimental system for measuring κ of GNPs is shown in Fig. 1. During the measurement, the powder was filled into a flat container after weighing and a tamper moved down to press against the powder to change the packing volume of the GNP powder. By cancelling out the weight of the container, the packing density of the GNP powder was calculated. A freestanding 3ω sensor consisting of a metal strip heater/thermometer encapsulated by two pieces of Kapton films was buried in the GNP powder to detect the κ of GNPs. A signal generator was used to provide a voltage signal driving the adjustable resistor and the metal strip in the freestanding 3ω sensor. A lock-in amplifier was utilized to detect and record the first and third harmonic voltage signals ($U_{1\omega}$ and $U_{3\omega}$, $U_{3\omega}/U_{1\omega}$ is typically 1/1000~1/500), which gave the temperature fluctuation variations of the encapsulated metal strip with adjustable current frequencies. The values of κ was deduced according to the following equations:[24-26]

$$\Delta T = -\frac{p}{2\pi l \kappa_{y,f}} \int_0^\infty \frac{1}{A_f B_f} \frac{\sin^2(b\lambda)}{(b\lambda)^2} d\lambda \qquad (1)$$

$$A_f = -\frac{\dfrac{\kappa_{y,s} B_s}{\kappa_{y,f} B_f} + \tanh(\eta_f)}{1 + \dfrac{\kappa_{y,s} B_s}{\kappa_{y,f} B_f} \tanh(\eta_f)} \qquad (2)$$

$$B_f = (\kappa_{xy,f} \lambda^2 + \frac{i2\omega}{a_{y,f}})^{1/2} \qquad (3)$$

$$B_s = (\lambda^2 + \frac{i2\omega}{a_{y,s}})^{1/2} \qquad (4)$$

$$\eta_f = B_f d_f \qquad (5)$$

$$\kappa_{xy,f} = \kappa_{x,f} / \kappa_{y,f} \qquad (6)$$

$$\Delta T_m = \frac{2U_{3\omega,rms}}{U_{1\omega,rms} \alpha_{CR}} \qquad (7)$$

Here, subscript x corresponds to the direction parallel to the Kapton film and sample interface (in plane), subscript y corresponds to the direction perpendicular to the Kapton film and sample interface (cross plane), subscript f denotes the Kapton film and subscript s represents the sample, subscript m corresponds to the experimental measurement. ΔT is the temperature rise, A and B are complex vectors, b is the strip half width, λ is the integrating factor, κ is the thermal conductivity, p/l is the peak electrical power per unit length, ω is the angular frequency of the alternating current, d is the thickness, η is the product of the thickness of each layer in the multilayer structure and the corresponding complex vector. κ_{xy} is the ratio of the in-plane to cross-plane thermal conductivity of the film, α is the thermal diffusivity, and α_{CR} is temperature coefficient of resistance (TCR) of the freestanding sensor, $U_{1\omega}$ is the measured first harmonic voltage and $U_{3\omega}$ is the measured third harmonic voltage. And all the voltages are root mean square (rms) values.

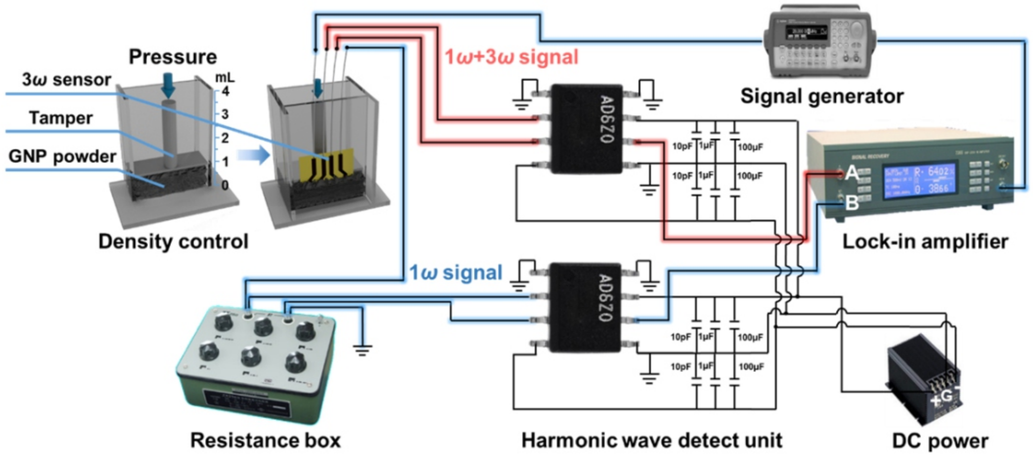

Fig. 1 Schematic diagram of the 3ω measurement system for nano-powders. The set-up consists of the freestanding 3ω sensor, density adjustable container, the signal generator (Agilent model 33220A) providing the reference signal for the commercial Lock-in amplifier (Ameteck Signal Recovery 7265), high-precision DC power source (Aerospace Changfeng Chaoyang Electrical Source Corp. 4NIC-X30), a pair of operational amplifiers (AD620), electric capacitors (10 pF, 1 lF and 100 lF) and adjustable resistance box (Shanghai Shuangte ZX25a).

3. Results and discussion

3.1 Scanning electron microscopy

SEM images exhibited the lamellar structures of GNP decorated with different metal or oxide NPs (Fig. 2a-e,i). The layered edges provided a clear evidence for that the GNPs were stacked with SL graphene. Oxide NPs were easier to observe because of their larger size than metal NPs. Energy-dispersive X-ray spectroscopy (EDX) of SiO_2 and Al_2O_3-decorated GNPs clearly confirmed that the atomic content of Si and Al from SiO_2 and Al_2O_3 NPs were at trace level (1.0 % and 0.3 %) in the selected areas (Fig. 2e,i). The element mapping was performed to reveal the element distribution for SiO_2 and Al_2O_3 on the selected area of GNP surface (Fig. 2f-h, j-l). These characterizations clarified the stacking structure of the graphene nanoplatelet and confirmed the presence of NPs.

3.2 Atomic force microscopy

As shown in Fig. 3, the height profiles (ΔZ) in the figure corresponded to the difference in the height between two points (Z_1, Z_2), which represented the thickness of the GNP. It was clearly seen that the thickness of GNPs was 4-9 nm, suggesting that approximately 4-9 layers of graphene consisted of the GNPs in the light of a SL graphene was 0.7-1.2 nm observed under AFM. Moreover, if the measurement points along a straight line were selected between the two ends of the GNPs, the lateral sizes of the six kinds of GNPs were estimated to be 300-500 nm.

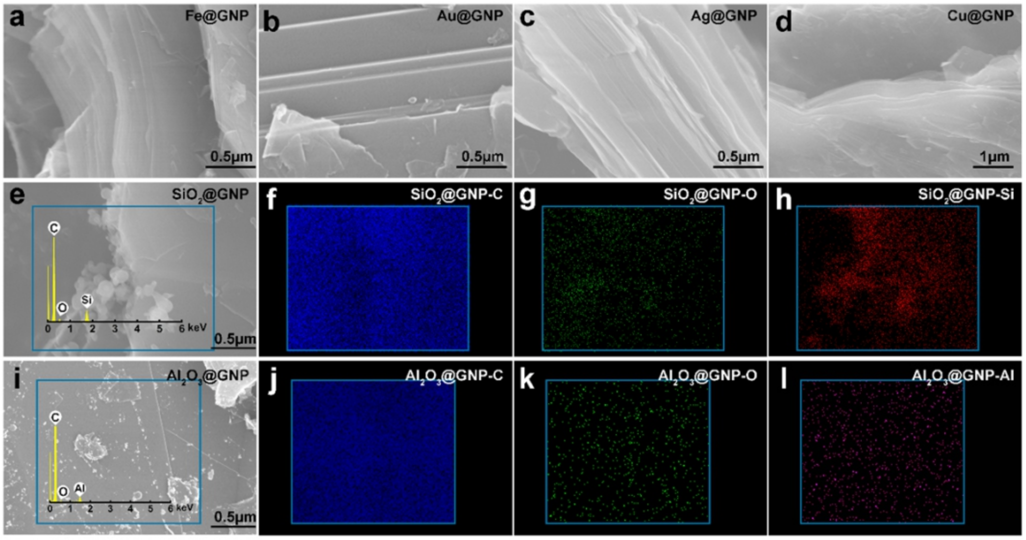

Fig. 2 **a-d**, Scanning electron microscopy (SEM) images showing the lamellar structures of GNP with different metal NPs (Fe, Au, Ag and Cu). **e**, **i**, SEM images showing the structures of GNP with oxide NPs (SiO_2 and Al_2O_3). Insets: energy-dispersive X-ray spectroscopy (EDX) for element analysis of the specific areas. **f-h**, Element mapping of C, O and Si corresponds to the selected area in sub-figure **e**. **j-l**, Element mapping of C, O and Al corresponds to the selected area in sub-figure **i**.

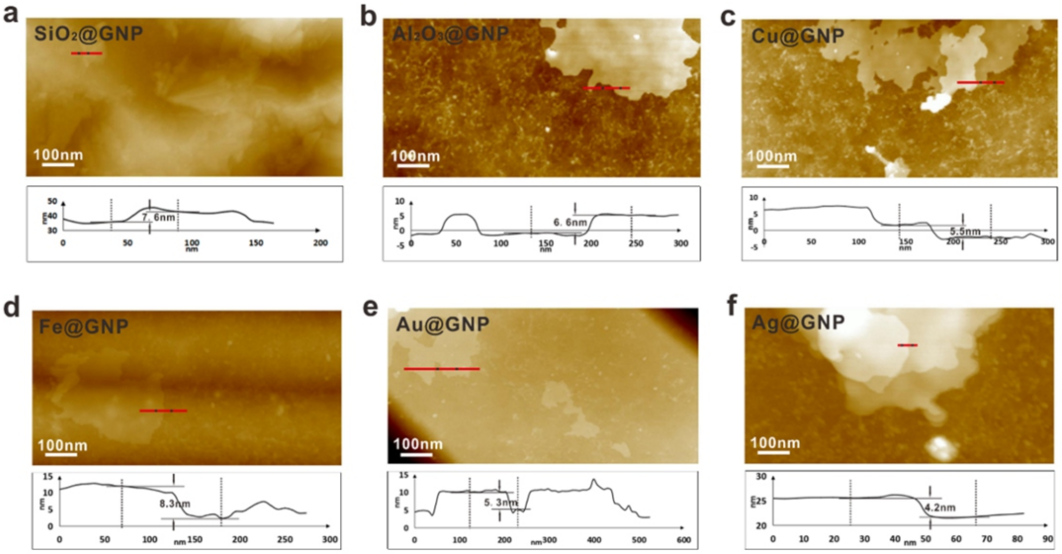

Fig. 3 Atomic force microscopy (AFM) images and the corresponding height profiles of the flake NP-decorated GNPs. The difference in height profiles between the two points indicates the thickness of the GNPs. The scan size is 1000 nm×500 nm and the data height range are 4-9 nm.

3.3 X-ray diffraction

We have further studied the effect of decorating NPs on the microstructure of GNPs using XRD. As shown in Fig. 4, after decoration of NPs, GNPs displayed a pronounced and sharp X-ray diffraction peak (002) at 26±1.0°, corresponding to a layer-to-layer distance (d_{002}) of about 0.324-0.345 nm, quite close to that of graphene layers in pristine graphite (0.335 nm, $2\theta = 26.6°$).[27] The values of out-of-plane coherence length (L_c) were calculated from the true Full Width Half Maximum (FWHM, β) of the (002) reflections using the Scherrer equation[27-30] by an analysis software, MDI jade. The results of d_{002} and L_c were summarized in Table 1. No characteristic diffraction peaks of NPs are observed because of its lower loading content and weak crystallization, which also implied that a good dispersion of the tiny NPs on the GNP surface.

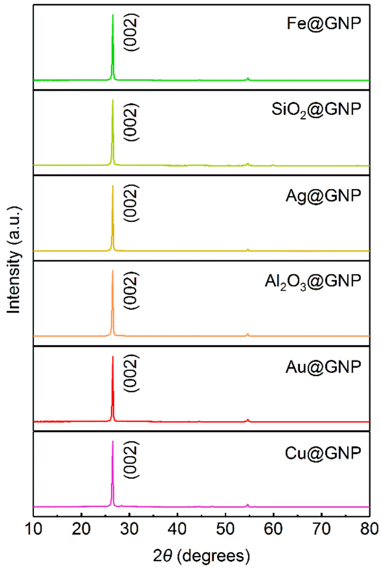

Fig. 4 X-ray diffraction (XRD) patterns of GNPs decorated with six kinds of NPs.

Table 1 Crystalline parameters for each GNP sample.

Sample Name	Peak(002)			
	2θ (degrees)	β (rad)	d_{002} (nm)	L_c (nm)
Fe@GNP powder	25.9	0.086	0.344	1.741
SiO_2@GNP powder	26.5	0.049	0.337	3.596
Ag@GNP powder	27.5	0.085	0.324	4.560
Al_2O_3@GNP powder	26.3	0.056	0.339	2.952
Au@GNP powder	26.5	0.058	0.336	3.128
Cu@GNP powder	25.8	0.038	0.345	3.890

3.4 Fourier transform infrared spectroscopy

FTIR was used to characterize the bonding information of various NP-decorated GNPs. GNPs mixed with KBr at a ratio of 1:100 (wt. %) were fabricated into tablets (diameter: 13 mm, thickness: 0.4 mm) for FTIR test. All of the six NP-decorated GNPs exhibited a peak occurring at about 1070 cm^{-1}, 1401 cm^{-1} and 1648 cm^{-1}(Fig. 5), which represented the C-O, C-O (carboxy) and C=C (aromatics) stretching vibrations, respectively. The occasional occurrence of O-H stretching vibration at about 3400 cm^{-1} was a reasonable result of absorbed vapor in the samples.[31,32] Notice that these peaks were the characteristic features of graphene. According to the Sadler's standard infrared spectrogram, the peaks at around 2920 cm^{-1} and 3121 cm^{-1} were caused by CH_2 symmetrical stretching vibration and NH_3^+. It was to be noted that CH_2 stretching vibration originated from graphene oxide. And if the preparation process of GNPs used hydrazine hydrate to reduce graphene oxide, NH^{3+} would also be introduced. In addition to chemical bonds and functional groups, the presence of metal nanoparticles attached onto the surface of graphene can also be validated via FTIR. Furthermore, some specific characteristic peaks representing the successful adhesion of NPs were found from FTIR spectra, including Fe-O (494 cm^{-1}), Si-O (1092 cm^{-1}), Ag (1578 cm^{-1}), Al-OH (909 cm^{-1}), Au (1060 cm^{-1}) and Cu-O (604 cm^{-1}) peaks.[33-35]

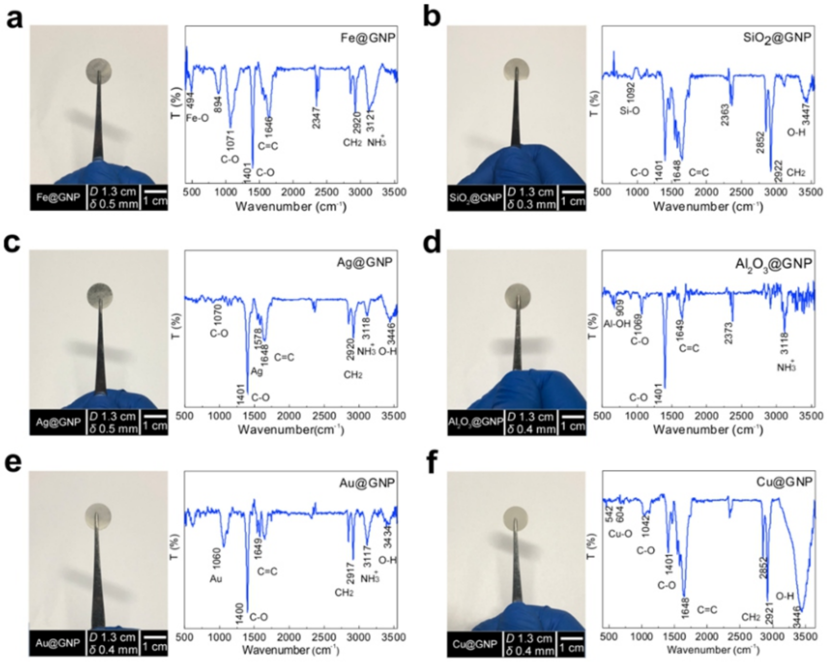

Fig. 5 Six kinds of NP-decorated GNP tablets used for FTIR test to characterize the chemical bonding information (left column) and the transmission spectra (right column) with the marked characteristic peaks.

3.5 Raman spectroscopy

The effect of different NP modification on the GNP load matrix was further examined by means of Raman spectroscopy. It was observed that under the identical excitation wavelength of 514 nm, the peak positions of *D*-band (~1350 cm^{-1}) and *G*-band (~1575 cm^{-1}) in different samples had no obvious shift (Fig. 6a), which means the modification of the NPs did not cause the phonons to softening or hardening.[36] By comparing the 2*D* peak of our GNPs with previously reported results at the same excitation wavelength, it was found that our GNPs were composed of 5 and 10 layers of graphene (Fig. 6b), which is consistent with the AFM results. The frequency-doubling mode 2*D* peak (*G*' peak) appeared at about 2707 cm^{-1}. Although this position of *G*' peak had a certain offset for different samples, the normalized intensity was basically the same (Fig. 6c), which reflects the quality and purity for the GNPs after NP decoration were nearly the same, owing to the fact that the intensity of *G*'-band is particularly sensitive to the sample purity as disorder would not allow for the coupling effect necessary for the two-phonon process.[37] The intensity ratio of the *D* peak and the *G* peak (I_D/I_G) is generally used to represent the quality of the graphene materials, and there is a linear relationship between this ratio and average crystalline size L_1. According to the results of Tuinstra and Koenig,[38] it was deduced that L_1 for our GNP samples was around 17-23 nm (Fig. 6d). In order to further study the effect of NPs on the thermal transport of GNPs, the relation between laser energy ($\mathcal{E}_L$) and *D* peak shift at different wavelengths was used to describe the dispersion relation of *D*-band (Fig. 6e). The slope values of each NP-decorated GNPs fluctuated over a range of $\partial\omega/\partial\varepsilon_L = 41\text{-}56\ cm^{-1}/eV$,[39] as shown in Table 2. The group velocity of transverse-acoustic (TA) phonon branch υ_{TA} in the long wavelength limit was estimated according to the relation $\upsilon_{TA} = \frac{\partial\omega}{\partial\Delta q} = \sqrt{3}a_0\gamma_0\frac{\partial\omega}{\partial\varepsilon_L}$.[39] It was clearly seen that decoration of different NP resulted in different phonon transmission velocities. Typically, Al_2O_3 and Fe NP-decorated GNPs exhibited the largest υ_{TA} (776 and 773 Å/cm) followd by Cu NP-decorated GNPs while Ag NP-decorated GNPs had the lowest υ_{TA} of 556 Å/cm. The values of υ_{TA} for Ag and SiO_2 NP-decorated GNPs were relatively moderate (658 and 612 Å/cm), suggesting that the decoration of different NPs would significantly affect the phonon transport within the stacking structure of GNP.

3.6 Thermal conductivity of NP-decorated GNP powder

It was intriguing to find that the values of κ of NP-decorated GNP powders are on the order of 0.1 W/m K (Fig. 7), which is extremely lower than the reported high κ of graphene. This could be explained by the fact that numerous fracture interfaces of GNPs compared with ideal 2D graphene interrupted the phonon transmission in pristine graphene layers, enabling the thermal transport properties greatly deviating from the excellent values of graphene. Moreover, the inter-layer decoration of NPs within GNPs provided extra phonon scattering sites, which reduced the mean free path of phonon transmission. Notice that κ increases with the increasing packing density, which is a conventional phenomenon widely exists in porous materials.[40]

According to the measured six samples, the κ value of Al_2O_3 NP-decorated GNPs was highest while that of the SiO_2 NP-decorated GNPs was lowest, and the results of the metal NP-decorated GNPs were close

Table 2 Summary of the slope values of the dispersion relation of *D*-band and the deduced group velocity of TA phonon branch.

	Au@GNP	Ag@GNP	Cu@GNP	Fe@GNP	Al_2O_3@GNP	SiO_2@GNP
$\partial\omega/\partial\varepsilon_L$($m^{-1}$/eV)	48	41	54	56	57	45
υ_{TA} (Å/cm)	658	556	741	773	776	612

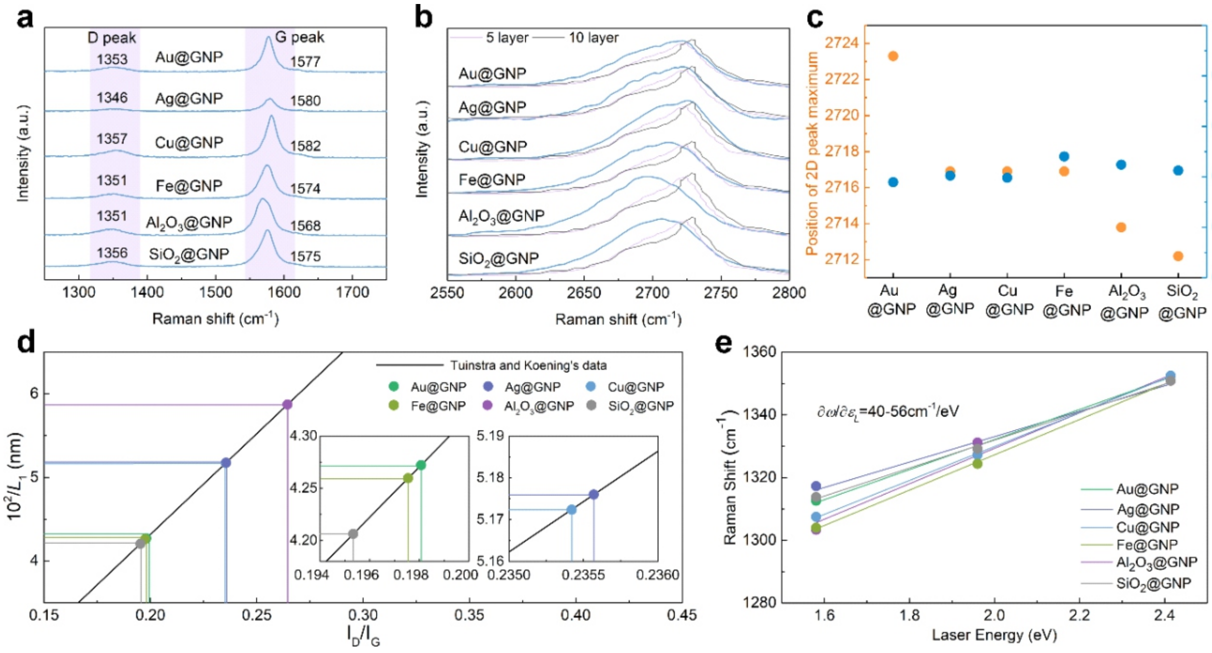

Fig. 6 Raman spectroscopy analysis of various NP-decorated GNPs. **a**, Raman spectra of six samples at an excitation wavelength of 514 nm. **b**, Comparison of 2D peak of our GNPs with previously reported 5 and 10 layers of graphene at an excitation wavelength of 514 nm.[37] **c**, The position shift (left axis) and normalized intensity (right axis) of 2D peak for different GNPs. **d**, Linear relation between the I_D/I_G ratio and $1/L_1$ (L_1 is average crystalline size) given by Tuinstra and Koenig[38] and our experimental data. **e**, Dependence of the frequencies of the D band on laser energy ($\mathcal{E}_L$) for different NP-decorated GNPs.

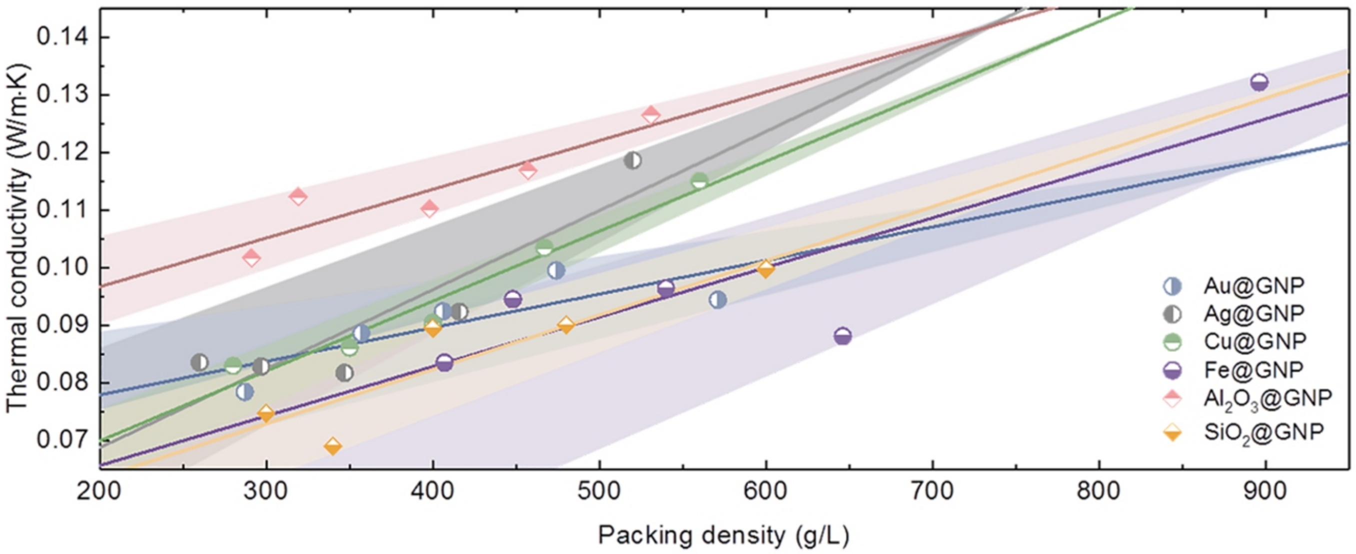

Fig. 7 Experimentally obtained thermal conductivity of various NP-decorated GNP powders versus packing density.

to each other. It can be obviously observed that the Al_2O_3 NPs were dispersed evenly onto the surface of the GNP, providing numerous evenly arranged channels facilitating the heat transfer between the graphene layers, and thus exhibited larger κ compared to other NP-decoration. In a marked contrast, the intercalated SiO_2 NPs enlarged the interlayer spacing and weakened van der walls force between graphene layers. The uneven distribution (Fig. 2) of SiO_2 NPs intercalated between graphene layers produced randomness of heat transfer, which resulted in the high level of mismatch of heat flux between adjacent GNP layers and impaired interlayer heat transfer efficiency. Owing to the fact that the concentration of Au, Ag, Cu and Fe NPs was too low to be accurately distinguished in SEM mapping, the thermal transport of the GNPs itself had not been influenced too much, which was clearly confirmed by the similar κ versus packing density trends as shown in Fig. 7.

4. Conclusion

In this study, we obtain extremely low thermal conductivity (~ 0.07 W/m·K) of stacking GNPs consisting of 4-10 layers of graphene by loading metal or non-metal NPs between graphene layers. This value is nearly 10^5 magnitudes lower than that of ideal 2D graphene materials, which is explained by the following two reasons. One is the incorporation of numerous fracture interfaces interrupts the phonon transmission in pristine graphite layers. The other is the inter-layer decoration of NPs within GNPs provides extra phonon scattering sites, greatly reducing the mean free path of phonon transmission. It is intriguing to observe that the alumina NP-decorated GNP has the largest phonon transport rate and thus has the highest thermal conductivity. While the uneven decoration of the silica NP increases the interlayer spacing so that the heat transfer ability is weakened between the graphene layers. When the content of NPs is small, the difference in the thermal conductivity due to the decoration with different NPs is not obvious. In a marked contrast, the thermal conductivity strongly depends on the stacking density of GNP powder, indicating using a small stacking density would be an effective approach to attain to extremely low thermal conductivity.

Acknowledgements

This research is supported by National Natural Science Foundation of China (Nos. 51876008 and 51876007) and the Fundamental Research Funds for the Central Universities from University of Science and Technology Beijing (Lin Qiu). Lin Qiu and Dongsheng Wen are grateful for the support from the Royal Society via its International Exchanges program.

References

1. K. S. Novoselov, A. K. Geim, S. V. Morozov, D. Jiang, M. I. Katsnelson, I. V. Grigorieva, S. V. Dubonos and A. A. Firsov, *Nature,* 2005, **438**, 197-200.
2. K. S. Novoselov, A. K. Geim, S. V. Morozov, D. Jiang, Y. Zhang, S. V. Dubonos, I. V. Grigorieva and A. A. Firsov, *Science,* 2004, **306**, 666-669.
3. Y. Zhang, J. P. Small, M. E. Amori and P. Kim, *Phys. Rev. Lett.,* 2005, **94**, 176803.
4. J. H. Chen, C. Jang, S. Xiao, M. Ishigami and M. S. Fuhrer, *Nat. Nanotechnol.,* 2008, **3**, 206-209.
5. M. D. Stoller, S. Park, Y. Zhu, J. An and R. S. Ruoff, *Nano Lett.,* 2008, **8**, 3498-3502.
6. Z. Qin, G. S. Jung, M. J. Kang and M. J. Buehler, *Sci. Adv.,* 2017, **3**, e1601536.
7. R. F. Service, *Science,* 2009, **324**, 875-877.
8. A. A. Balandin, S. Ghosh, W. Bao, I. Calizo, D. Teweldebrhan, F. Miao and C. N. Lau, *Nano Lett.,* 2008, **8(3)**, 902-907.
9. K. Saito, J. Nakamura and A. Natori, *Phys. Rev. B,* 2007, **76(11)**, 115409.
10. F. Yavari, H. R. Fard, K. Pashayi, M. A. Rafiee, A. Zamiri, Z. Yu, R. Ozisik, T. Bora-Tasciuc and N. Koratkar, *J. Phys. Chem. C,* 2011, **115(17)**, 8753-8758.
11. P. Goli, S .Legedza, A. Dhar, R. Salgado, J. Renteria and A. A. Balandin, *J. Power Sources,* 2014, **248**, 37-43.
12. L. W. Fan, X. Fang, X. Wang, Y. Zeng, Y. Q. Xiao, Z. T. Yu, X. Xu, Y. C. Hu and K. F. Cen, *Appl. Energ.,* 2013, **110**, 163-172.
13. M. Mehrali, E. Sadeghinezhad, S. T. Latibari, S. N. Kazi, M. Mehrali, M. N. B. M. Zubir and H. S. C. Metselaar, *Nanoscale Res. Lett.,* 2014, **9(1)**, 15.
14. F. Wang, L. T. Drzal, Y. Qin and Z. Huang *J. Mater. Sci.,* 2015, **50(3)**, 1082-1093.
15. M. T. Hung, O. Choi, Y. S. Ju and H. T. Hahn. *Appl. Phys. Lett.,* 2006, **89(2)**, 023117.
16. C. Liu, K. Wang, S. Luo, Y. Tang and L. Chen, *Small,* 2011, **7(9)**, 1203-

1206.
17. Y. K. Kim, H. K. Na and D. H. Min, *Langmuir,* 2010, **26(16)**, 13065-13070.
18. K. Jasuja and V. Berry, *ACS Nano,* 2009, **3(8)**, 2358-2366.
19. J. Li and C. Liu, *Eur. J. Inorg. Chem.*, 2010, **2010(8)**, 1244-1248.
20. W. Hong, H. Bai, Y. Xu, Z. Yao, Z. Gu and G. Shi, *J. Phys. Chem. C,* 2010, **114(4)**, 1822-1826.
21. R. Wang, Z. Wu, C. Chen, Z. Qin, H. Zhu, G. Wang, H. Wang, C. Wu, W. Dong, W. Fan and J. Wang, *Chem. Commun.,* 2013, **49(74)**, 8250-8252.
22. G. M. Scheuermann, L. Rumi, P. Steurer, W. Bannwarth and R. Mülhaupt, *J. Am. Chem. Soc.,* 2009, **131(23)**, 8262-8270.
23. Z. Xu, H. Gao and G. Hu, *Carbon*, 2011, **49(14)**, 4731-4738.
24. L. Qiu, D. W. Tang, X.H. Zheng and G. P. Su, *Rev. Sci. Instrum.,* 2011, **82(4)**, 045106.
25. L. Qiu, X. H. Zheng, G. P. Su, D and W. Tang, *Int. J. Thermophys.,* 2013, **34(12)**, 2261-2275.
26. L. Qiu, N. Zhu, H. Y. Zou, Y. H. Feng, X. X. Zhang and D. W. Tang, *Int. J. Heat Mass Tran.,* 2018, **125**, 413-433.
27. H. L. Guo, X. F. Wang, Q. Y. Qian, F. B. Wang and X. H. Xia, *ACS Nano,* 2009, **3(9)**, 2653-2659.
28. N. Iwashita, C. R. Park, H. Fujimoto, M. Shiraishi and M. Inagaki, *Carbon,* 2004, **42(4)**, 701-714.
29. L. Qiu, X. T. Wang, D. W. Tang, X. H. Zheng, Norris P M, D. S. Wen, J. N. Zhao, X. H. Zhang and Q. W. Li, *Carbon,* 2016, **105**, 248-259.
30. L. Qiu, X. H. Zheng, J. Zhu, G. Su and D. W. Tang, *Carbon,* 2013, **51**, 265-273.
31. E. Y. Choi, T. H. Han, J. Hong, J. E. Kim, S. H. Lee, H. W. Kim and S. O. Kim, *J. Mater. Chem.,* 2010, **20(10)**, 1907-1912.
32. N. Kurantowicz, E. Sawosz, S. Jaworski, M. Kutwin, B. Strojny, M. Wierzbicki, J. Szeliga, A. Hotowy, L. Lipińska, R. Koziński, J. Jagiełło and A. Chwalibog, *Nanoscale Res. Lett.,* 2015, **10(1)**, 23.
33. S. S. Shankar, A. Rai, A. Ahmad and M. Sastry, *J. Colloid Interf. Sci.,* 2004, **275(2)**, 496-502.
34. P. Yuan, F. Annabi-Bergaya, Q. Tao, M. Fan, Z. Liu, J. Zhu, H. He and T. Chen, *J. Colloid Interf. Sci.,* 2008, **324(1-2)**, 142-149.
35. D. Zhang and Z. Zhan, *J. Alloy. Compd.,* 2016, **654**, 226-233.
36. F. Tuinstra and J. L. Koenig, *J. Chem. Phys.*, 1970, **53(3)**, 1126-1130.
37. R. A. DiLeo, B. J. Landi and R. P. Raffaelle, *J. Appl. Phys.,* 2007, **101(6)**, 064307.
38. F. Tuinstra, J. L. Koenig., *J. Compos. Mater.,* 1970, **4(4)**, 492-499.
39. M. J. Matthews, M. A. Pimenta, G. Dresselhaus, M. S. Dresselhaus and M. Endo, *Phys. Rev. B,* 1999, **59(10)**, R6585.
40. L. Qiu, H. Y. Zou, D. W. Tang, D. S. Wen, Y. H. Feng and X. X. Zhang, *Appl. Therm. Eng.,* 2018, **130**, 1004-1011.